Spin Transfer and Magnetic Interaction via Phosphorus in Nitronyl Nitroxide Radical-Substituted Triphenylphosphine Derivatives

Corinne Rancurel,[†] Henrike Heise,[‡,§] Frank H. Köhler,*[,‡] Ulrich Schatzschneider,[||] Eva Rentschler,*[,⊥,#] Jose Vidal-Gancedo,[+] Jaume Veciana,*[,+] and Jean-Pascal Sutter*[,†]

Institut de Chimie de la Matière Condensée de Bordeaux − CNRS, Université Bordeaux 1, 87 Ave. Dr. Schweitzer, F-33608 Pessac, France, Anorganisch-chemisches Institut, Technische Universität München, D-85747 Garching, Germany, California Institute of Technology, Pasadena, California 91125, Max-Planck-Institut für Bioanorganische Chemie, Stiftstrasse 34-36, D-45470 Mülheim an der Ruhr, Germany, and Institut de Ciència de Materials de Barcelona, Campus Universitari de Bellaterra, E-08913 Cerdanyola, Spain

Received: January 19, 2004

The magnetic behavior of polyradicals is usually understood on the basis of the spin polarization scheme displayed by the molecules. As far as conjugated hydrocarbon species are concerned, the spin distribution is rather well established and follows the sign alternation principle. Yet when a heteroatom is involved in the exchange pathway, the situation may become more delicate. This study concerns the involvement of a P-atom in the spin distribution and the intramolecular exchange interaction of nitronyl nitroxide radical-substituted triphenyl phosphine derivatives. The spin distribution of mono-, bi-, and tri-radical phosphine derivatives has been investigated by high-resolution fluid solution EPR and ^{1}H and ^{31}P MAS NMR spectroscopy. These techniques permitted one to establish that spin density is located at the phosphorus atom and showed that its sign depends on whether there is a P-lone pair or not. They also revealed the spin polarization scheme for the molecules. While these schemes are in line with ferromagnetic interaction between the radical units, the actual interactions are extremely weak as found by the magnetic studies. The experimental data are supported by DFT computations (UB3LYP/Lanl2DZ), which reproduce very well the effective spin distribution on these molecular systems except the sign inversion observed when going from the phosphine to its phosphine oxide counterpart. They also predict a very small high-spin/low-spin gap for these polyradicals.

Introduction

The search for new magnetic materials based on paramagnetic molecules assembled into supramolecular architectures is currently a topic of intensive effort. Especially an approach involving persistent aminoxyl radicals has become a challenging research area for chemists. Together with purely organic assemblies of radicals,[1−3] heterospin systems which consist of paramagnetic metal ions linked by organic radicals acting as ligands attract much attention.[4−10] Following this strategy, the use of polyradical species as bridging ligands allowed the synthesis of molecule-based magnets with ordering temperatures of up to 46 K.[11,12] The development of this promising approach, however, depends on the design of new paramagnetic polydentate ligands that will permit one to modulate both the architectures and the magnetic properties of these supramolecular species.

A prerequisite for obtaining materials with a permanent magnetization by this organic-π/metal-d (or f) spin strategy is that the organic linker possesses a magnetic ground state, ideally a high-spin ground state in the case of polyradicals. A convenient approach to predict the sign of the intramolecular exchange interactions, that is, ferro- or antiferromagnetic, in π-conjugated polyradicals is based on the polarized π-spin principle. Indeed, the spin delocalization starting from a radical moiety, an aminoxyl group for instance, over the core of the molecule leads to a pattern that reflects the polarization of the bonding electrons. Thus, two neighboring atoms will bear excess α-spin (positive spin) and β-spin (negative spin) density, respectively, and this sign alternation is spread over the whole molecule. When the molecule contains a second radical moiety, two situations can be encountered. Either the spin-distribution schemes of both radical moieties lead to the same sign of the spin density at the linker atoms, and then the exchange interaction between the radical moieties is predicted to be ferromagnetic, or the polarization induced by one radical moiety is opposite to the polarization induced by the other, and the exchange interaction is anticipated to be antiferromagnetic. This easy-to-handle predictive tool was efficiently applied to the design of numerous conjugated hydrocarbon polyradical species. When this approach to high-spin molecules was extended to polyradicals linked through a heteroatom, it appeared that the nature of the heteroatom, and especially whether it has a lone pair or not, could play a crucial role in the effective intramolecular exchange interaction by modifying the spin distribution scheme.[13,14]

Our contribution to this topic concerns the possibility of using open-shell phosphine derivatives as building blocks for magnetic

* Corresponding authors. E-mail: jpsutter@icmcb.u-bordeaux1.fr (J.P.S.), f.h.koehler@lrz.tu-muenchen.de (F.H.K.), rentschler@uni-mainz.de (E.R.), vecianaj@icmab.es (J.V.).

[†] Institut de Chimie de la Matière Condensée de Bordeaux.

[‡] Technische Universität München.

[§] Present address: Max-Planck-Institut für biophysikalische Chemie, Am Fassberg 11, D-37077 Göttingen, Germany.

[||] California Institute of Technology.

[⊥] Max-Planck-Institut für Bioanorganische Chemie.

[#] Present address: Institut für Anorganische und Analytische Chemie, Universität Mainz, Germany.

[+] Institut de Ciència de Materials de Barcelona.

10.1021/jp049730+ CCC: $27.50
Published on Web 06/16/2004

SCHEME 1: Synthesis Pathway for the Preparation of 1d,e, 2d, and 3d

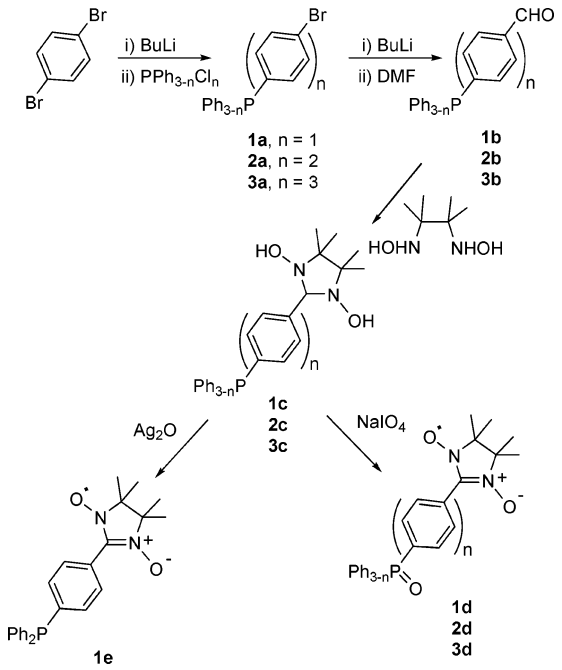

materials. These compounds comprise a triphenylphosphine core substituted by a 4,4,5,5-tetramethyl-4,5-dihydro-1*H*-imidazolyl-1-oxy-3-oxide radical moiety, hereafter abbreviated as nitronyl nitroxide radical. Two of such monosubstituted phosphine derivatives have already been briefly described.[15] These were shown to be able to coordinate to a metal center by means of either the phosphorus atom[16−18] or the aminoxyl unit.[19,20] The presence of two phenyl groups available for further substitution prompted us to envisage the corresponding polyradical derivatives. Herein, we report on the synthesis and magnetic characteristics of a series of mono-, di-, and tri-*p*-nitronyl nitroxide triphenylphosphine derivatives.

The aim of this work was to evaluate the potential of a P atom in mediating the exchange interaction between the aminoxyl radicals it bridges. The role played by the phosphorus atom in the intramolecular exchange interaction and more generally the complete understanding of the magnetic behavior shown by these molecules require the knowledge of the spin density distributions over the molecules. Fluid solution high-resolution EPR[21] and NMR[22] spectroscopy have proven to be very efficient tools for assessing the magnitude and sign of the spin density borne by the atoms of organic open-shell molecules. These techniques appeared ideally suited for the compounds envisaged in the present study because all atoms of the molecular fragment linking the radical units are active nuclei in NMR and EPR, that is, ^{1}H, ^{13}C, and ^{31}P. The experimental investigations performed were complemented by DFT computational studies and both confirm that the heteroatom in the bridging position contributes to the spin distribution.

Results

The nitronyl nitroxide-substituted phosphine derivatives considered in this study are the mono-*p*-nitronyl nitroxide triphenylphosphine, **1e**, and its oxide, **1d**, as well as the di- and tri-*p*-nitronyl nitroxide triphenylphosphine oxides, **2d** and **3d** (Chart 1).

In the following, we will first briefly describe their preparation and characterization; in the second part, we will investigate the spin distributions for these molecules by high-resolution EPR and MAS NMR spectroscopies and then their magnetic properties will be considered, and, finally, our experimental results will be compared to the computational data on these and related compounds.

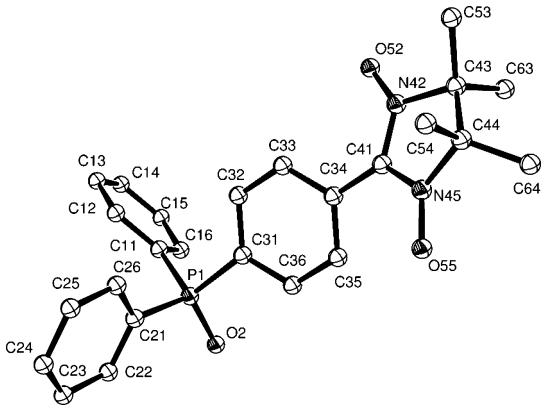

Figure 1. ORTEP plot (30% probability ellipsoids) of the molecular structure for compound **1d** (the hydrogen atoms are omitted for clarity).[15] Selected bond lengths (Å) and angles (deg): P1−O2, 1.485-(2); O52−N42, 1.275(3); 055−N45, 1.279(3); C41−N42, 1.352(3); C41−N45, 1.350(3); substituted phenyl C−C, 1.378−1.399; C31−P1−O2, 111.4(1); C33−C34−C41−N42, 28.3(2).

Synthesis. The compounds **1d,e**−**3d** were prepared according to the synthesis pathway described by Scheme 1. The first step consists of the synthesis of the corresponding *para*-aldehyde-substituted phenylphosphines, **1b**−**3b**. These are efficiently obtained in a two-step procedure. The mono-lithiation of *p*-dibromobenzene with ^{n}BuLi followed by the reaction with PCl_nPh_{3-n} ($n = 1-3$) yields the corresponding *p*-bromophenylphosphine, **1a**−**3a**.[23,24] The reaction of **1a**−**3a** with ^{n}BuLi and its subsequent formylation by reaction with DMF leads to **1b**−**3b** in good yields. Except derivative **2b**, these compounds were already obtained previously by alternative procedures.[25−28] The mono-, di-, and tri-radical phosphine oxide derivatives, **1d**−**3d**, are prepared in standard fashion[29] by condensation of the corresponding aldehyde with 2,3-dimethyl-2,3-dihydroxyaminobutane followed by oxidation with $NaIO_4$ under phase-transfer conditions. The use of a periodate salt as oxidant results in the formation of both the radical and the phosphine oxide in a single step. For the preparation of phosphine **1e**, a milder and selective oxidant is required. We have shown that a selective formation of the radical can be obtained if Ag_2O is used as oxidant.[16]

X-ray Structure Characterization. An X-ray crystallographic analysis could be performed for the mono-radical phosphine oxide derivative **1d**, and its solid-state structure has already been described.[15] A view of the molecular structure and selected geometrical features are recalled in Figure 1. The structure of phosphine derivative **1e** has been confirmed indirectly by the adduct $\{Mo(CO)_5(\mathbf{1e})\}$, **4**, formed by its coordination to the $Mo(CO)_5$ fragment and has been reported.[16]

High-Resolution Isotropic EPR. Electron paramagnetic resonance (EPR) has proven to be a powerful spectroscopic technique yielding detailed information about the electronic structure of open-shell molecules. When performed in dilute fluid solutions under high-resolution conditions, EPR measurements provide precise isotropic hyperfine coupling constants for nuclei with both large and small spin densities.[21] The value of the hyperfine coupling observed by EPR is directly related to the absolute spin density on the considered nucleus. The X-band EPR spectra of compounds **1d**−**3d** were recorded in degassed CH_2Cl_2 solutions ($<10^{-4}$ M). The spectrum obtained

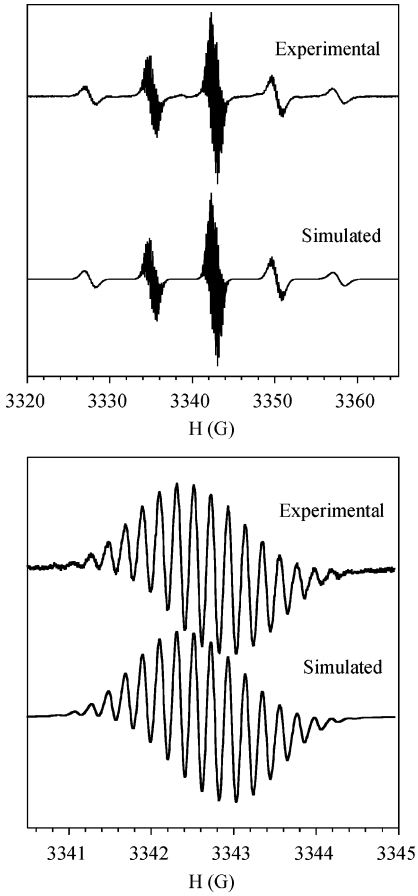

Figure 2. Experimental and simulated EPR spectrum of the mono-radical compound **1d** (top); details of the central group of lines (bottom). The best simulation parameters are $a_N = 7.543$ G (2N), $a_P = 0.597$ G (1P), $a_{Hmethyl} = 0.205$ G (12H), $a_{Hortho} = 0.450$ G (2H), and $a_{Hmeta} = 0.190$ G (2 H).

for the mono-radical **1d** at 230 K is centered at $g = 2.006$ and consists of five equally spaced groups of signals with an intensity ratio of 1:2:3:2:1 due to the coupling of the unpaired electron with two equivalent ^{14}N nuclei of the nitronyl nitroxide unit. Each of these main signals is composed of a large number of lines due to further coupling with the magnetically active nuclei of the compound, that is, ^{1}H and ^{31}P. Figure 2 shows the spectrum of compound **1d** under high-resolution conditions together with the simulated signals. This simulation required one to consider hyperfine couplings with two equivalent N nuclei and the 12 equivalent H nuclei of the nitronyl nitroxide unit along with the H in the ortho and meta positions of the substituted phenyl group (see Chart 1 for the labeling) and the P nucleus. The values for the isotropic hyperfine coupling constants found by simulation of the experimental spectrum of **1d** are given in Table 1. The resulting line width, $\Delta H_{1/2}$, for the protons and phosphorus was 0.109 G, and for the nitrogen it was considered as $\Delta H_{1/2} = 0.109 + 0.29m_i - 0.046m_i^2$, where m_i stands for the nuclear spin, to take into account slow molecular tumbling effects. The observation of a single set of 12 equivalent H's for the methyl groups of the radical unit results from a rapid exchange in solution of the axial and equatorial positions for the CH_3 groups of the five-membered heterocycle. The spin transfer to the phenyl ring is revealed by the couplings found with the aromatic H atoms; moreover, the observation of a coupling with the P nuclei indicates that a degree of spin is also located on this atom.

The high-resolution spectra for the di-radical, **2d**, and the tri-radical, **3d**, derivatives centered at $g = 2.006$ are reproduced

CHART 1

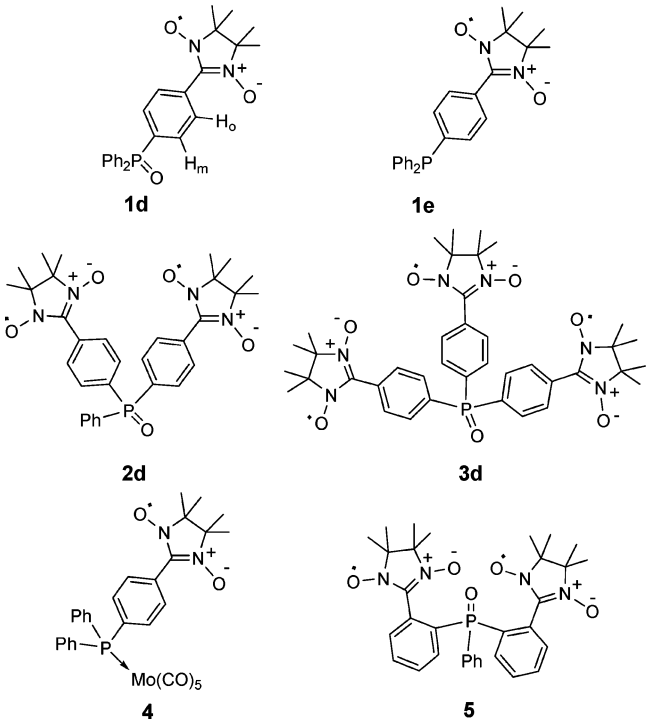

in Figure 3. They consist of, respectively, 9 and 13 main signals regularly spaced with visible coupling constants of $a_N = 3.77$ G and $a_N = 2.51$ G (line-to-line separation), respectively. These coupling constants are one-half and one-third of the observed a_N for mono-radical **1d**. In addition, the multiplicities of the spectra are in agreement with the number of lines expected for the coupling to four (**2d**) and six (**3d**) equivalent N nuclei as a result of intramolecular spin−spin exchange interactions between the radical units.[30] Therefore, the observed patterns point out clearly that the exchange interaction is much larger than the hyperfine interaction ($|J| \gg |a_N|$).

The experimental lines recorded for **2d** and **3d** are broadened, as compared to those of compound **1d**. Moreover, for **2d** it can still be seen that each main signal is composed of several poorly resolved lines, while they are no longer visible for compound **3d**. For an individual molecule **2d** or **3d**, the inter-radical distance is not so large, and hence the observed line broadening is probably due to dipolar interactions. In addition, the visible hyperfine coupling constants of the di- and tri-radicals are smaller than those of the mono-radical, which could result in line overlap. This line broadening prevents the determination of the hyperfine coupling constants for the other magnetically active nuclei that are smaller than a_N for compounds **2d** and **3d**.

The high-resolution EPR spectra obtained for compounds **1d**−**3d** in fluid solutions are in agreement with the formulation as mono-, di-, and tri-radicals, respectively. More importantly, they suggest that spin density is located on the H atoms of the substituted phenyl groups and on the P atom as found by the simulation of the spectrum of compound **1d**. To gather more information on the spin distribution in these molecules, we considered another spectroscopic method, solid-state MAS NMR spectroscopy.

Spin Density Distribution by ^{1}H and ^{31}P MAS NMR Spectroscopy. Solid-state magic angle spinning NMR spectroscopy has recently been shown to be a powerful alternative to polarized neutron diffraction for mapping the distribution of the spin density in paramagnetic molecular and supramolecular solids.[31−33] This technique provides information on both the

TABLE 1: Contact Shifts (δ^{con}, in ppm), Hyperfine Coupling Constants (a in G), and Spin Densities (ρ in au $\times 10^{-3}$) Obtained from High-Resolution EPR[a] and Solid-State NMR[b] Spectroscopies

		compound					
		1d (EPR)	**1d** (NMR)	**2d** (NMR)	**3d** (NMR)	**1e** (NMR)	Mo(**1e**)$(CO)_5$ (NMR)
CH_3	δ^{con}		−13.0	−15.1	−15.8	*c*	−11.5/−17.3[d]
	α	0.205	−0.174	−0.203	−0.211		−0.154/−0.232
	ρ	±0.13	−0.11	−0.13	−0.13		−0.10/−0.15
H_o	δ^{con}		35.5	33.2	41.0	*c*	33.8
	α	0.450	0.476	0.445	0.550		0.453
	ρ	±0.28	0.30	0.28	0.34		0.28
H_m	δ^{con}		−12.4	−11.4	−12.5	*c*	−7.4
	α	0.190	−0.166	−0.153	−0.168		−0.099
	ρ	±0.13	−0.10	−0.10	−0.11		−0.06
C_6H_5	δ^{con}		0.4	0.2		*c*	0.3
	α	<0.01	<0.01	<0.01			<0.01
	ρ	∼0	∼0	∼0			∼0
N	α	7.543	*c*	*c*	*c*	*c*	*c*
P	δ^{con}		103.6	212.3	324.9/359.7	−94.9	21.9
	α	0.597	0.563	1.154	0.563/1.955	−0.516	0.119
	ρ	±0.93	0.87	1.79	2.73/3.03	−0.80	0.18

[a] In CH_2Cl_2 at 230 K. [b] For measuring conditions, see Experimental Section and Supporting Information. [c] Not measured. [d] Axial and equatorial methyl groups resolved.

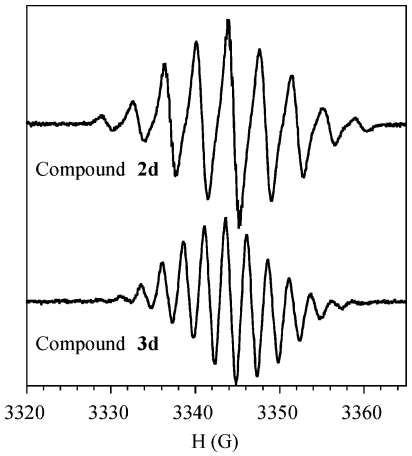

Figure 3. Experimental high-resolution EPR spectra for di-radical **2d** and tri-radical **3d** recorded in CH_2Cl_2 at 250 K.

value and the sign of the spin density of the magnetically active nuclei. It appeared especially adapted for the investigation of the spin density not only located at the protons but also at the P atom because the ^{31}P isotope has a nuclear spin of $I = {}^1/_2$ and 100% natural abundance.

The ^1H MAS NMR spectra of the solid mono-, **1d**, and tri-radical, **3d**, are shown in Figure 4. In the bottom spectrum, three isotropic signals are assigned to the tri-radical. The methyl protons of the nitronyl nitroxide unit appear at −14.1 ppm, and the protons in the ortho and meta positions (H_o and H_m) of the phenyl groups are seen at 47.0 and −4.5 ppm, respectively. An additional isotropic peak near −244 ppm in both spectra is due to nickelocene, which has been used for internal calibration of the temperature in much the same way as described previously.[34] For compound **1d** (top spectrum), the methyl signal at −11.4 ppm shows some structure, pointing to axial and equatorial methyl groups. There are two separate signals for the methyl groups of {Mo(**1e**)$(CO)_5$}, **4**, while in other cases, these signals are not resolved,[31] and the same is true for **3d**. The protons H_o and H_m of **1d** appear, respectively, at 41.7 ppm (as a shoulder of the first high-frequency sideband of the methyl signals) and at −4.5 ppm as a shoulder of the methyl signal, respectively. The additional signal at 7.9 ppm belongs to the nonresolved protons of the unsubstituted phenyl groups at the phosphorus

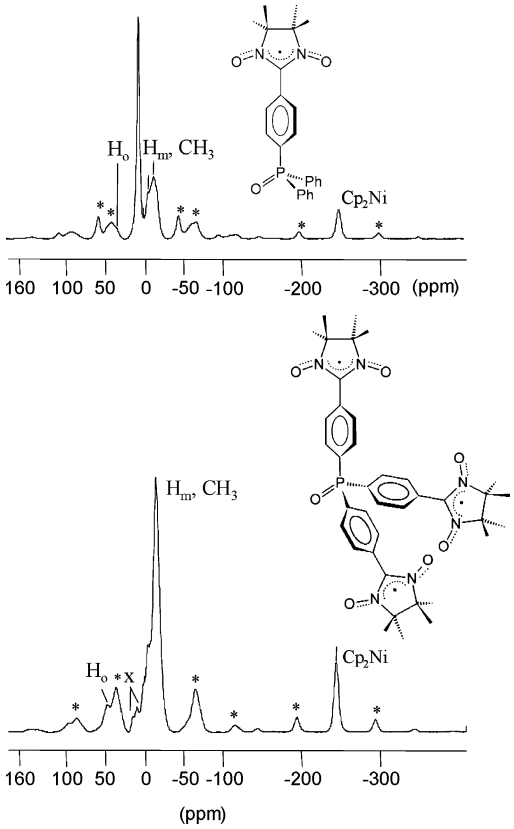

Figure 4. ^1H MAS NMR spectra of mono-radical **1d** (top) and tri-radical **3d** (bottom) (T = 309 K, spinning rate 15 kHz). Spinning sidebands are marked by asterisks, and the signals due to an impurity are marked by X. The proton signal of Cp_2Ni is used as the internal temperature standard.

atom. The ^1H MAS NMR spectra of **2d** and **4** not shown in Figure 4 have been analyzed accordingly.

Conversion of the experimental signal shifts into contact shifts, δ^{con} (see Experimental Section) and further into the hyperfine coupling constants, a(X), of the nucleus X by using eq 1 gave the data collected in Table 1. In eq 1, γ_X is the nuclear gyromagnetic ratio, h and k are the Planck and Boltzmann constants, respectively, T is the absolute temperature, g is the isotropic g-factor, β_E is the Bohr magneton, and S is the spin

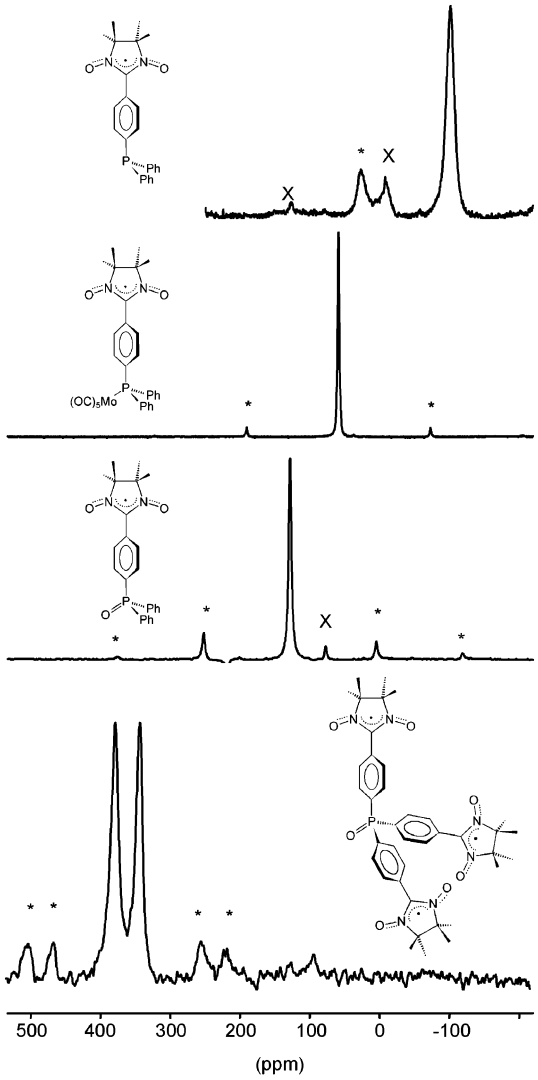

Figure 5. ^{31}P MAS NMR spectra from top to bottom: mono-radical phosphine, **1e** (T = 308 K, spinning rate 15 kHz), its molybdenum derivative **4** (T = 308 K, spinning rate 12 kHz), and the phosphine oxide derivatives, **1d** and **3d** (both T = 309 K, spinning rate 15 kHz). Spinning sidebands are marked by asterisks, and the signals due to an impurity are marked by X.

quantum number. The contact shifts were also converted into the spin densities, ρ(X) at the nucleus X by means of eq 2, where μ_0 is the vacuum permeability, and a_0 is the Bohr radius, while the other symbols have been mentioned with eq 1. The spin densities are also given in Table 1.

$$a(\mathrm{X}) = \frac{3\gamma_{\mathrm{X}} hkT}{g^2\beta_{\mathrm{E}}{}^2 S(S+1)}\,\delta^{\mathrm{con}} \qquad (1)$$

$$\rho(\mathrm{X}) = \frac{9kT}{\mu_0 g^2 \beta_{\mathrm{E}}^2 a_0{}^3 (S+1)}\,\delta_T^{con} \qquad (2)$$

The ^{31}P MAS NMR spectra have been recorded for all compounds. While ^{31}P NMR data in solution have been obtained only for phosphino-substituted *N*-oxides,[35] solid-state ^{31}P MAS NMR data of organic radicals do not seem to be known. The overall trends of the spectra are shown in Figure 5 for compounds **1e**, **1d**, **3d**, and **4**. For both phosphines and phosphine oxides, sharp signals (half widths 0.6−1.7 kHz) and small shift anisotropies are found. Hence, favorable signal resolution and signal-to-noise ratios enable even small impurities

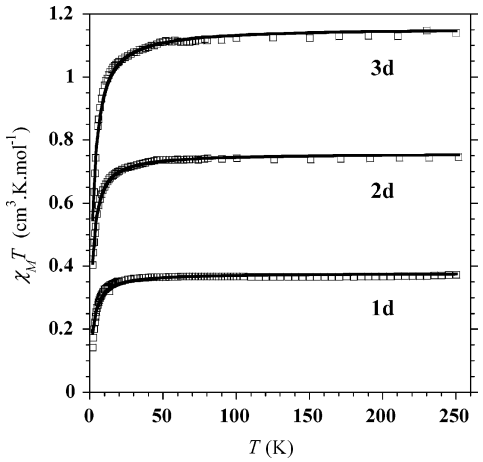

Figure 6. Experimental (□) and calculated (−) magnetic behavior for compounds **1d**, **2d**, and **3d** in the solid state.

to be detected (see spectra of **1e** and **1d** in Figure 5), which would be hard to uncover by other means. More importantly, two signals at 341.4 and 374.9 ppm are resolved for pure **3d**, indicating two independent molecules in the asymmetric unit. This has been confirmed by the spectrum of **3d** dissolved in CD_2Cl_2 (saturated with TEMPO to shorten the electron relaxation time), which shows only one ^{31}P NMR signal at 381 ppm. It is worth noting that ^{31}P MAS NMR is more efficient than ^{1}H MAS NMR spectroscopy, which does not provide such details.

Magnetic Properties. *Solid-State Properties.* The temperature dependence of the molar magnetic susceptibility, χ_{M}, for compounds **1d**,**e**, **2d**, and **3d** was measured on polycrystalline samples in the temperature range 2−300 K using a SQUID magnetometer. The results, plotted as $\chi_{\mathrm{M}}T$ versus T in Figure 6, show that for each compound $\chi_{\mathrm{M}}T$ remains invariant in the temperature range 300−50 K with values in agreement with the presence of one, two, and three independent $S = {}^1/_2$ spin carriers per molecule, respectively. Below 50 K, $\chi_{\mathrm{M}}T$ decreases to reach a value of 0.14 cm^3 K mol^{-1} for **1d**, 0.12 cm^3 K mol^{-1} for **1e**, and 0.4 and 0.5 cm^3 K mol^{-1} for **2d** and **3d**, respectively, at 2 K.

For all compounds, the solid-state magnetic behavior at low temperature is governed by overall antiferromagnetic interactions. For mono-radical **1d** and **1e**, this behavior can only result from intermolecular magnetic interactions. The crystal structure available for **1d** indicates that several short intermolecular separations involving the aminoxyl units exist in the solid.[15] The shortest distances are found for O52 (x, y, z) and C54 ($^1/_2 - x$, $^1/_2 + y$, $^1/_2 - z$) with 3.447(4) Å, O55 (x, y, z) and C54 (1 + x, y, z) with 3.440(4) Å, the closest O52 (x, y, z)−O55 ($^3/_2 - x$, y, z) separation being 4.785(3) Å; they reveal a complex network of short intermolecular contacts that could be responsible for the observed antiferromagnetic interactions. To evaluate the strength of the magnetic interactions for these compounds, the magnetic data were analyzed by considering a Curie−Weiss behavior. A best fit to the experimental data yielded values of θ = −2.07 K for **1d**, −2.48 K for **1e**, −1.71 K for **2d**, and −2.20 K for **3d**. These values indicate that the overall interactions in the solid state are very similar for all compounds; no evidence is found for the possible contribution of intramolecular interactions for the polyradical derivatives. To investigate the intramolecular contribution, frozen matrix EPR studies were undertaken.

Frozen Matrix EPR. The frozen matrix for the di- and triradical **2d** and **3d** was formed from 10^{-3} M CH_2Cl_2−toluene (1:1) solutions. The spectra recorded for both compounds at 10

TABLE 2: Comparison of Selected Distances for the Optimized Geometries and X-ray Structure for Compound 1d

bond	X-ray structure	optimized at 6-31G (C, H, N)/6-31+G* (P, O) level	optimized at Lanl2DZ level
P1−O2	1.482(2)	1.506	1.614
P1−C11	1.797(2)	1.829	1.871
P1−C21	1.795(2)	1.829	1.871
P1−C31	1.806(2)	1.830	1.870
N42−O52	1.275(3)	1.288	1.324
N45−O55	1.279(3)	1.287	1.323

K exhibit a broad line (ca. 40 G peak-to-peak) centered at $g = 2.006$, in which the dipolar fine structure is not resolved. This broad line corresponds to the $\Delta m_S = 1$ transition among sublevels of the triplet state. A signal at $g = 4$ corresponding to the $\Delta m_S = 2$ transition, characteristic of triplet and quartet species, became visible only below 10 K and remained weak for lower temperatures. The signal at $g = 6$ corresponding to the $\Delta m_S = 3$ transition which is characteristic for the quartet state of tri-radical derivatives was not detected for compound **3d**, but this forbidden transition is seldom observed.[36−38] Because the $\Delta m_S = 2$ transition was observed as a weak signal only below 10 K, the ground state could not be assessed from the temperature dependence of the signal intensity. Nevertheless, it follows that the intramolecular exchange interaction must be very weak for both compounds. In an effort to gain complementary information on these compounds, DFT calculations of the spin density distribution and intramolecular exchange interaction were carried out.

Theoretical Calculations. *Optimized Geometry*. Comparison of the optimized geometry of mono-radical **1d** to its crystallographic structure shows that the calculations done with the Lanl2DZ basis set are generally in good agreement, although the N−O, P−C, and P−O bonds are systematically too long. The geometry optimization was repeated using a 6-31G (C, H, N)/6-31+G* (P, O) basis because the 6-31+G* basis set also includes diffuse functions said to be advantageous for calculations on compounds with lone pairs. Indeed, the inclusion of diffuse functions leads to geometrical parameters for **1d** in better agreement with the structural data (see Table 2). However, the spin densities calculated with the Lanl2DZ basis set showed much better agreement with the experimental values regardless of the basis set used for optimization (see below), so only the latter was used throughout for both optimizations and calculation of the spin density.

Spin Densities. The spin density distributions calculated with the X-ray coordinates and with the optimized geometry for mono-radical **1d** are virtually identical to those found for a large number of other nitronyl nitroxide derivatives investigated with most of the spin density located on the N−O groups (1.2597 and 1.2815 au, respectively, for the X-ray and optimized structures) and a negative contribution from the central C2 (C41 Figure 1) carbon atom, −0.2410/−0.2421 au (X-ray/opt.), due to spin polarization effects.[39] The phenyl ring bearing the radical group carries small additional spin densities with the normal alternating pattern (Table 3), while there is virtually no spin density on the nonsubstituted rings ($<\pm 0.0002$ au). The spin densities at the P and O atoms are 0.0007/0.0017 au (X-ray/opt.) and −0.0004/−0.0006 au (X-ray/opt.), respectively.

This compound also served as a test case to compare the influence of the geometry and basis set on the spin density distribution. The results obtained using different basis sets for geometry optimization and calculation of the spin density are collected in Table 3. The spin density at the phosphorus atom

TABLE 3: Comparison of the Spin Density Distributions Found for the Mono-radical 1d as a Function of the Basis Sets Used

optimized at: spin density at:	Lan12DZ Lanl2DZ	Lan12DZ 6-31G/ 6-31+G*	6-31G/ 6-31+G* Lanl2DZ	6-31G/ 6-31+G* 6-31G/ 6-31+G*
P1	0.0017	0.0003	0.0013	−0.0003
O2	−0.0006	−0.0005	−0.0006	−0.0003
C31 (P−C)	−0.0534	−0.0543	−0.0535	−0.0542
C32 (meta)	0.0317	0.0343	0.0311	0.0337
C33 (ortho)	−0.0587	−0.0603	−0.0576	−0.0593
C34 (C−NIT)	0.0635	0.0711	0.0635	0.0712
C35 (ortho)	−0.0584	−0.0602	−0.0569	−0.0587
C36 (meta)	0.0316	0.0343	0.0310	0.0337
C41 (NIT C2)	−0.2421	−0.2547	−0.2437	−0.2556
N42	0.2672	0.3023	0.2685	0.3044
O52	0.3701	0.3376	0.3700	0.3432
N45	0.2656	0.3007	0.2672	0.3032
O55	0.3786	0.3460	0.3770	0.3365

at the 6-31G/6-31+G* level is systematically smaller than that calculated at the Lanl2DZ level and deviates much more from the experimental values deduced from EPR and NMR experiments than for the latter case. When 6-31G/6-31+G* is also used for the geometry optimization, the sign of the spin density even turns negative on P1, in contrast to the experimental results. On the other hand, the Lanl2DZ spin densities do not deviate significantly regardless of at which level the geometry was optimized (columns 2 and 4, Table 3). Therefore, it seems justified to use the Lanl2DZ basis set for both geometry optimization and spin density calculations.

The spin density distribution in the di-radical derivative **2d** is very similar to that of **1d**, as revealed by the resemblance of values for all nuclei of nitronyl nitroxide and *p*-phenylene units obtained for the triplet state of **2d** and for mono-radical **1d** (Tables S2a and S4a of the Supporting Information). In line with this result, the values resulting for P and O of **2d**, 0.0033 and −0.0012 au, respectively, are twice those for the corresponding P and O nuclei of **1d** because each of the two radical moieties contributes simultaneously to the spin polarization on both atoms. The low-spin state (singlet) for **2d** shows all of the necessary characteristics of the broken-symmetry open-shell state with the pattern of spin density on one of the phenyl-radical moieties reversed when compared to that of the triplet (Table S4a of the Supporting Information), and the P and O atoms depleted in spin density, with calculated values of 0.0000 au on both atoms. For the high-spin state (quartet) of tri-radical **3d**, the spin density distributions on all three phenyl-radical moieties are almost identical and close to those of the mono- and di-radicals (Table S5a of the Supporting Information). The spin density on the three phenyl rings is virtually identical, and the P and O atoms carry spin densities of 0.0049 and −0.0019 au, respectively.

The spin density distribution for the phosphine derivative **1e** is virtually identical to that of its phosphine oxide counterpart, **1d**, with the phosphorus atom carrying a spin density of 0.0008 au (Table S3a of the Supporting Information). The same picture is obtained when the corresponding hypothetical di- and tri-radicals phosphine derivatives are considered (see Tables S6a and S6c of the Supporting Information). For the two latter compounds, the calculated spin density at P is found to be positive with 0.0017 and 0.0033 au, respectively.

Exchange Coupling Parameters. The exchange coupling constant calculated for the phosphine oxide di-radical **2d** is very small and antiferromagnetic with $J = -0.2$ cm^{-1}; a similar exchange parameter is obtained for the phosphine analogue **2e** with $J = -0.4$ cm^{-1}. The extremely small differences in energy

between the open-shell singlet and triplet states preclude any definitive conclusion as to whether the P atom acts as a ferro- or antiferromagnetic coupler. This situation probably reflects the small spin density on the core of the molecule linking the nitronyl nitroxide units as well as the intramolecular separation, that is, the number of atoms between the two magnetic centers. To gain further information on the exchange interaction via a P atom, we considered the case of the di-radical **5** (Chart 1) with the two radical units bound to phosphorus in the ortho position of the phenyl group because it is well known that ortho and para isomers of di-radicals usually show the same type of magnetic exchange interactions if the geometries are comparable.[40] The shorter link between the aminoxyl units was anticipated to lead to a more significant singlet−triplet energy gap, providing more reliability in the theoretical computations. Calculations using X-ray structural coordinates for compound **5** revealed that the two phenyl rings bearing the nitronyl nitroxide groups carry small spin densities (Table S7a of the Supporting Information) as anticipated from the large phenyl-radical dihedral angles.[41] Very little spin density is found on PO, 0.0044 and −0.0051 au for P and O, respectively. The pattern of the spin density distribution derived from the optimized geometry and the X-ray structure is very similar, and the absolute values show only small differences, although the spin density on the two phenyl rings is somewhat larger for the former (X-ray, 0.1738; calc., 0.1989), most likely reflecting the smaller torsion angles between the phenyl and imidazolidine rings at the optimized geometry (52.1° (calc.) versus 67.4° (X-ray) and 62.8° (calc.) versus 72.7° (X-ray)). The spin density distribution in the low-spin state at both the X-ray structure and the optimized geometry is virtually identical to that of the corresponding triplet states. The reversed sign on one of the phenyl-radical moieties shows that the calculation converged to the open-shell broken-symmetry singlet state and not to a charge-transfer closed-shell singlet state. It can be noticed that the spin density on P and O atoms is depleted and becomes negative in the broken symmetry state (P: −0.0009 and −0.0003 au. X-ray/opt.) as compared to that in the triplet state (P: 0.0044 and 0.0036 au. X-ray/opt.).

The exchange interaction parameter calculated for the X-ray structure points to an extremely weak antiferromagnetic exchange with $J = -0.15\ cm^{-1}$. However, the exchange parameter found for the optimized geometry is positive and 1 order of magnitude larger with $J = 1.87\ cm^{-1}$. This difference might be attributed to the smaller torsion angles found between the nitronyl nitroxide moieties and the phenyl groups in the optimized geometry as compared to the X-ray structure. Indeed, the spin transfer is favored by the former geometry as pointed out by the calculations (vide supra), and the intramolecular exchange becomes operative.

Discussion

There are two main issues associated with the experimental results. (i) How is the magnetic information delocalized from the spin sources NO of the nitronyl nitroxide to an atom, like P, that can serve as a donor? (ii) How do nitronyl nitroxides interact magnetically when they are linked by a phosphorus atom? The first question is of course related to the fact that the magnetic interaction of a paramagnetic ligand with a paramagnetic transition metal center would decisively depend on the sign and amount of spin density at the donor atom. In the present case, inspection of the proton NMR data in Table 1 shows that the spin delocalization from the nitronyl nitroxide moiety into the phenyl group proceeds via spin polarization, as evidenced by the alternating sign of the spin density on the ortho and meta protons. It is gratifying that good agreement between EPR, NMR, and DFT data is found, in particular that there is more (positive) spin density at H_o than (negative) at H_m. This is in line with previous EPR,[21] NMR,[31,42,43] and polarized neutron diffraction[44] results. Continuing the spin polarization path along the phenyl skeleton, one would expect positive spin density at the phosphorus atom in the para position, and this was indeed found for the phosphine oxide derivatives **1d**, **2d**, and **3d**. In this series, the spin density at phosphorus (and oxygen) increases with the number of radical moieties bound to the P atom (see Table 4). The slight deviations from linear correlation on going from **1d** to **3d** might be due to small changes of the geometries as a result of differences in the steric crowding. The proportionality observed between the spin population on P and the number of nitronyl nitroxide units may be understood by considering that a single C-atom induces spin density on P for mono-radical **1d** whereas two and three are operative for the di-radical **2d** and tri-radical **3d**, respectively. Moreover, it strongly suggests that the spin density located on P arises exclusively from the intramolecular distribution, while neighboring radical molecules in the crystal lattice have a negligible contribution to the spin population.

TABLE 4: Comparison of the Experimental and Computed (Lanl2DZ Basis Set) Spin Densities

	calculated spin density at O ($\rho_{\alpha-\beta}$ in au × 10^{-3})	calculated spin density at P ($\rho_{\alpha-\beta}$ in au × 10^{-3})	experimental spin density at P ($\rho_{\alpha-\beta}$ in au × 10^{-3})
1d	−0.6 (−0.4)[a]	1.7 (0.7)[a]	0.87
2d	−1.2	3.3	1.78
3d	−1.9	4.9	2.73/3.02
1e	*c*	0.8	−0.80
2e	*c*	1.7	*b*
3e	*c*	3.3	*b*
5	−3.4 (−5.1)[a]	3.6 (4.4)[a]	*b*

[a] In brackets, calculated values with the X-ray structure. [b] Not available. [c] No oxygen atom.

Quite strikingly, there is a change to negative spin density at phosphorus when passing from the phosphine oxide **1d** to the phosphine derivative **1e**. As this may be due to the involvement of the phosphorus lone pair in the spin transfer, we have investigated the compound {Mo(**1e**)$(CO)_5$}, **4**, where the lone pair is blocked by donor bond formation to the Lewis-acidic $Mo(CO)_5$ fragment. Actually, this also entails a shift to positive spin density at phosphorus, although the effect is not as pronounced as for the phosphine oxides (see Table 1). From the synthetic point of view, this means that, by varying the Lewis acidity of a transition metal fragment, the chemist may tune the sign and amount of spin at donor atoms such as phosphorus, nitrogen, and the like. If the transition metal fragment is also paramagnetic, it should be possible to thereby tune the magnetic interaction between the ligand radical and the metal center.

The change of the sign of the spin on phosphorus has a parallel in the behavior of nuclear coupling constants. The reason is that, by measuring paramagnetic NMR signal shifts, one actually observes electron−nuclear couplings, which are usually dominated by the Fermi contact interaction in much the same way as internuclear couplings.[45] Thus, on passing from Me_3P to Me_3PO, the reduced ^{31}P, ^{13}C coupling constant changes from −11.1 to 55.8 N A^2 m^{-3}, respectively.[46,47] For the pair $(Me_3Sn)_3P$ and $[(Me_3Sn)_3P]Cr(CO)_5$, the reduced ^{119}Sn, ^{31}P coupling constant shifts from −456 to −224 N A^2 m^{-3}.[48] Note that the reduced coupling constants were used here to eliminate the different signs of the gyromagnetic ratios of ^{13}C and ^{119}Sn.

SCHEME 2: Schematic Drawing of the Contributions Inducing the Spin Polarization on P[a]

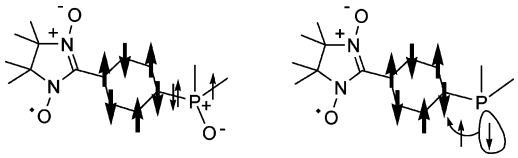

[a] The bold ↑ represents the spin polarization mediated by the π-electrons, and the thin ↑ represents the spin polarization of the electrons of the σ-bonds or of the lone pair.

Again, the result is that, upon engaging the phosphorus lone pair in bonding, the coupling is gradually shifted to more positive values. Depending on the strength of the bonding, this does or does not lead to a sign reversal.

To account for the sign of the spin density at phosphorus and its reversal when passing from phosphine to phosphine oxide derivatives, two contributions likely to lead to the spin polarization on P can be invoked. These contributions arise from the polarized π-electrons of the phenyl rings and those of the C−P σ-bonds.[22] A phosphine oxide derivative lacks π-electrons located on P, and a realistic canonical form of the PO bond can be drawn as P^+-O^-.[49] The spin polarization is thus exclusively induced by the electrons of the C−P σ-bonds. For the compounds considered in this study, a negative spin density is located on the C atom bound to P. Therefore, a positive spin density is anticipated on P (Scheme 2a), and this is indeed found experimentally. The σ-contribution applies as well for the phosphines, but obviously for these derivatives another contribution involving the lone pair imposes a negative spin on P. Here, a hyperconjugation leading to the mixing of some electron density of the phosphorus lone pair with the aromatic π-system might be operative (Scheme 2b). The limit situation depicted in Scheme 2b has no reality with phosphorus but is well established for related oxygen or nitrogen derivatives and is at the origin of the super-exchange mechanism.[50−52] Nevertheless, a small contribution of this type cannot be excluded for the phosphorus derivatives.

Thus, for a phosphine oxide derivative, the linking P atom is spin polarized through the σ contribution, and the spin polarization scheme over the whole molecule should be in agreement with the sign alternation principle; the same is true for a phosphine coordinated to a metal center. However, when the phosphorus possesses a lone pair, this principle does not apply anymore and the spin on the heteroatom is imposed through the polarization of the lone pair by the aromatic π-system. The occurrence of this latter contribution was not expected for phosphorus derivatives (vide infra).

The spin density distributions deduced from DFT calculations are in good agreement with the distribution obtained experimentally; the values on P for all compounds are compared in Table 4. A discrepancy, however, exists between the calculated and experimental data for phosphine **1e** because the computations do not reproduce the sign reversal of the spin density at P upon passing from **1d** to **1e** due to the lone-pair effect discussed above. This is likely due to limits in the basis set employed, which is unable to accurately reproduce this through-space interaction. However, the calculations do reflect the above-mentioned trend to a more positive spin density when the lone pair is engaged in a bond.

Turning to the second initial question about magnetic exchange interaction between phosphorus-linked nitronyl nitroxides, there is general interest in this topic. While this work was in progress, aminoxyl radicals which are connected by a Si,[53] B, C, and N atoms[54] and more generally by E atoms[55] were reported. On the basis of strictly topological considerations, the phosphine polyradical derivatives considered here should lead to ferromagnetic interactions. Moreover, for the phosphine oxide derivatives, the spin polarization schemes found experimentally are in complete agreement with the polarization alternation anticipated for ferromagnetic exchange among the radical units of a molecule. The presence of spin density at P is also a clear indication that the bridging atom does not shield the intramolecular magnetic interactions. However, the magnetic studies performed for **2d** and **3d** did not permit one to evidence intramolecular exchange because Curie behaviors are observed down to low temperatures suggesting extremely small exchange interactions between the radical units. Such a behavior is supported by the DFT calculations. The computed energy differences between the high-spin and low-spin states are found to be so small that they preclude any conclusion on whether ferro- or antiferromagnetic exchange should be operative. The fact that no exchange interaction was observed in the temperature domain investigated could reflect the rather feeble spin population on the core of the molecules. The nitronyl nitroxide unit is know to poorly polarize the molecular fragment it is connected to.[56] Moreover, all of the compounds considered in this study are "doubly disjoint" systems; that is, the radical-phenyl moieties are connected to the phosphorus by a carbon-atom bearing negative spin density. Thus, at the bridge, the C-atoms with substantial positive spin density are separated by three atoms of feeble spin densities ($C_{para}-P-C_{para}$), and this will further deplete the intramolecular exchange interaction.[57,58]

The effect of structural and geometrical parameters on the strength of the exchange coupling is confirmed by the calculation performed for the *ortho*-di-radical derivative **5** for which the two spin carriers are connected through less atoms. Experimentally, this compound has been found to exhibit a very weak antiferromagnetic intramolecular interaction, if any, between the radical units.[40] This behavior was attributed to the dihedral angles close to 90° between the radical moieties and the phenyl groups they are linked to, angles which preclude spin transfer from the radical units. A weak antiferromagnetic interaction ($J = -0.15$ cm^{-1}) is indeed found by the calculations reported here. Yet, more interestingly, when a geometry with reduced angles is considered, a ferromagnetic exchange ($J = 1.87$ cm^{-1}) is found. The results obtained for **5** support our assumption that the weakness of the intramolecular exchange interactions for the para nitronyl nitroxide derivatives considered above is certainly related to the poor spin polarization of the core of the molecule linking the magnetic units.

Further information on the electronic structure of these nitronyl nitroxides derivatives is obtained from the orbital energies and characters for compounds **1d** and **1e** as representatives of the phosphine oxide and phosphine series. With regard to the magnetic orbitals, both radicals show the "normal" pattern with two almost degenerate α-HOMOs and slightly higher lying β-LUMOs centered on the NO groups of the five-membered rings. On the other hand, in both cases, P- or PO-centered virtual orbitals were found to be much higher in energy (for **2d**: α-LUMO+8, β-LUMO+10). This energy gap certainly is a handicap in the mixing of the magnetic orbitals through the central heteroatom[59] and may account, together with the rather small spin population found on the core of the molecules, for the extremely weak exchange interactions found for these nitronyl nitroxide phosphine derivatives. An increase of the

strength of the interaction via the P might be obtained by replacing the nitronyl nitroxide unit by a radical ensuring for a better delocalization of the unpaired electrons on the whole molecule.[60]

Concluding Remarks

The information gathered for the series of mono-, bi-, and tri-nitronyl nitroxide-substituted phosphine derivatives unambiguously establishes that the bridging P atom is involved in the spin distribution exhibited by the molecules. The presence of spin density at phosphorus supports the occurrence of an intramolecular exchange pathway between the spin carriers, and both the experimental spin polarization scheme deduced from MAS NMR studies and the computed scheme suggest a high-spin ground state for the polyradical derivatives. However, according to magnetic measurements, the effective exchange interactions were too weak to be investigated experimentally. Finally, for the phosphine derivatives, the lone pair of the heteroatom was anticipated to have minor effects due to its poor mixing with the aromatic π-orbitals. Actually, the sign of the spin density at P depends dramatically on whether there is a P lone pair or not. A correlation between the sign of the spin density on P and the spin ground state of such a polyradical remains to be established. This will require phosphine derivatives with increased exchange interactions between the spin carriers, compounds that are also desirable in a perspective of use as building blocks for the preparations of molecule-based magnets.

Experimental Section

Synthesis. Commercially available solvents and reagents were used throughout without further purification, except for those mentioned below which were purified as described. The (4-bromophenyl)diphenylphosphine, **1a**,[23] and 2,3-dimethyl-2,3-dihydroxyamino-butane[61,62] were prepared following described procedures. Dry THF was obtained by distillation from Na/benzophenone, CH_2Cl_2 was distilled from CaH_2, MeCN was dried over P_2O_5, DMF was dried over $MgSO_4$ and distilled under vacuum, and MeOH was dried over $Mg(OMe)_2$ prior to distillation. Reactions involving *n*-BuLi were carried out under N_2 using oven-dried glassware. PPh_2Cl, $PPhCl_2$, and PCl_3 were distilled prior to use. Solution NMR spectra were recorded on a Bruker instrument operating at 200 MHz for ^1H; chemical shifts (δ) are given in ppm. Infrared spectra were recorded in the range 4000−400 cm^{-1} using a Perkin-Elmer FT-IR Paragon 1000. Elementary analysis was performed by the "Service Central d'Analyze du CNRS" at Vernaison, France.

Di-(4-bromophenyl)diphenylphosphine 2a. A solution of *p*-dibromobenzene (7.0 g, 29.7 mmol) in THF (20 mL) was added dropwise over a period of 1 h to a solution of *n*-BuLi (1.6 M in hexane; 18.5 mL; 29.7 mmol) kept at −65 °C. Afterward, neat PCl_2Ph (2 mL) was slowly added, and the reaction mixture was stirred at room temperature for 8 h. After hydrolysis with H_2O (15 mL), the organic phase was extracted with Et_2O, washed with H_2O until the aqueous phase had a pH = 7, and dried over Na_2SO_4. The solvent was removed in vacuo, leading to **2a** (3.76 g, yield = 60%) as an oil that was used without further purification for the next step. Analyses data for this compound are consistent with the literature.[24]

Tri-(4-bromophenyl)phosphine 3a. This compound was prepared as described for **2a**.[24]

(4-Formylphenyl)diphenylphosphine 1b. A solution of **1a** (5.0 g; 14.7 mmol) in THF (20 mL) was added dropwise over a period of 1 h to a solution of *n*-BuLi (1.6 M in hexane; 9.2 mL; 14.7 mmol) kept at −70 °C, followed by a solution of DMF (1.36 mL; 17.6 mmol) in THF (20 mL). The reaction mixture was then stirred 10 h at room temperature. Afterward, H_2O (15 mL) was cautiously added, and the mixture was extracted with CH_2Cl_2. The organic layer was washed with H_2O and dried over Na_2SO_4 before the solvent was removed in a vacuum. The resulting oil was crystallized from MeOH, yielding **1b** (3 g, yield = 63%) as a white crystalline solid. An alternative synthesis for this compound was reported earlier.[63] IR (KBr): 1705 (s), 1592 (m), 1432 (m), 1208 (m), 1088 (w), 825 (s), 748 (s), 695 (s).

^1H NMR ($CDCl_3$, 293 K, ppm): δ = 10.0 (s, 1H, CHO); 7.55 (m, 14H, Ar.).

Di-(4-formylphenyl)phenylphosphine 2b. This compound was prepared by the same procedure as **1b**, yielding **2b** (yield 70%) as an oil used without further purification. ^1H NMR ($CDCl_3$, 293 K, ppm): δ = 10.0 (s, 2H, CHO); 7.70 (m, 13H, Ar).

Tri-(4-formylphenyl)phosphine 3b. This compound was prepared by the same procedure as **1b**, yielding **3b** (60%) as an oil which was used without further purification. ^1H NMR ($CDCl_3$, 293 K, ppm): δ = 10.0 (s, 3H, CHO); 7.70 and 7.20 (m, 12H, Ar).

4′-[2-(1,3-Dihydroxy-4,4,5,5-tetramethylimidazoline)-phenyl]diphenylphosphine 1c. A solution of **1b** (2.23 g, 77 mmol) and 2,3-dimethyl-2,3-dihydroxyaminobutane (1.2 g, 81 mmol) in MeOH (40 mL) was refluxed for 12 h in a N_2 atmosphere. The resulting precipitate was filtered and washed with MeOH, yielding **1c** as a white solid (1.9 g, yield = 60%).

IR (KBr): 3421 (s), 2988 (m), 2914 (m), 1434 (m), 1377 (m), 1146 (m), 1113 (m), 797 (m), 742 (s), 696 (s), 516 (m). ^1H NMR ($CDCl_3$, 293 K, ppm): δ = 7.35 (m, 14H, Ar); 5.15 (s broad, OH); 4.71 (s, 1H, CH); 1.08 (s, 12H, CH_3). ^{31}P NMR ($CDCl_3$, 293 K, ppm): δ = −5.49 (s).

Di-{4′-[2-(1,3-dihydroxy-4,4,5,5-tetramethylimidazoline)-phenyl]}phenylphosphine 2c. A solution of **2b** (0.43 g, 1.35 mmol) and 2,3-dimethyl-2,3-dihydroxyaminobutane (0.4 g, 2.7 mmol) in MeOH (10 mL) was refluxed for 12 h in a N_2 atmosphere. After being cooled to room temperature, the reaction mixture was filtered and the volume of the filtrate was reduced to ca. 4 mL. Addition of H_2O (20 mL) induced the precipitation of a white solid. The latter was collected by filtration, washed with H_2O, and dried in vacuo, yielding **2c** (0.58 g, yield = 70%). ^1H NMR (DMSO-d_6, 293 K, ppm): δ = 7.78 (s broad, 4H, OH); 7.30 (m, 13H, Ar); 4.50 (s, 2H, NCH); 1.06 and 1.03 (2s, 24H, Me).

Tri-{4′-[2-(1,3-dihydroxy-4,4,5,5-tetramethylimidazoline)-phenyl]}phosphine 3c. This compound was obtained following the same procedure as for **2c,** leading to **3c** (0.67 g, yield = 63%) as a white solid. ^1H NMR ($CDCl_3$, 293 K, ppm): δ = 7.77 (s broad, 6H, OH); 7.50 and 7.20 (m, 12H, Ar); 4.50 (s, 3H, NCH); 1.06 and 1.03 (2s, 24H, Me).

4′-[2-(1-Oxyl-3-oxide-4,4,5,5-tetramethylimidazoline)-phenyl]diphenylphosphine Oxide 1d. A solution of $NaIO_4$ (0.150 g, 0.68 mmol) in H_2O (10 mL) was added to a suspension of **1c** (0.22 g, 0.46 mmol) in CH_2Cl_2 (20 mL). The reaction mixture was stirred for 10 min, during which a deep blue color developed in the organic phase. The latter was collected, washed with H_2O, and dried over Na_2SO_4 before the solvent was removed in vacuo. The residue was purified by chromatography over neutral Al_2O_3 (1.3 × 12 cm, eluent CH_2Cl_2−acetone 4/1). The main blue band was collected, the solvent was removed in vacuo, and the residue was dissolved in Et_2O, leading to the formation of deep blue crystals of **1d** (0.12 g, yield = 60%).

Anal. Calcd for $C_{25}H_{26}N_2O_3P$: C, 69.27; H, 6.05; N, 6.46. Found: C, 68.98; H, 6.20; N, 6.20. UV−vis {MeOH, λ (nm) (ϵ)}: $\lambda = 588$ (351); 373 (8975); 273 (13 057). IR (KBr): 1437 (m), 1420 (m), 1389 (m), 1364 (s), 1193 (s), 733 (w), 714 (m), 692 (m), 546 (s). EPR (CH_2Cl_2, 293 K): $g = 2.006$ (5 lines, $a_N = 7.5$ G); powder sample, $g_{||} = 2.006$; $g_\perp = 2.009$.

4′-[2-(1-Oxyl-3-oxide-4,4,5,5-tetramethylimidazoline)-phenyl]diphenylphosphine 1e. A suspension of **1c** (0.10 g, 0.24 mmol) and Ag_2O (83 mg, 0.35 mmol) in CH_2Cl_2 (20 mL) was stirred at room temperature, and the reaction evolution was characterized by the development of a blue color followed by TLC (SiO_2, CH_2Cl_2; **1e**, $R_f = 0.8$; **1d**, $R_f = 0$). The reaction was stopped by filtration over Celite as soon as traces of **1d** were detected. The solvent was removed in vacuo, and the residue was dissolved in Et_2O from which **1e** crystallized as a blue solid (70 mg, yield = 70%). Anal. Calcd for $C_{25}H_{26}N_2O_2P$: C, 71.93; H, 6.28; N, 6.71. Found: C, 72.04; H, 6.36; N, 6.60. UV−vis {CH_2Cl_2, λ (nm) (ϵ)}: $\lambda = 632$ (357); 595 (357); 375 (10 357); 300 (14 430); 272 (14 570). IR (KBr): 2985 (w), 1434 (m), 1419 (s), 1388 (m), 1368 (s), 1303 (m), 1131 (m), 1089 (m), 697 (s). EPR (CH_2Cl_2, 293 K): $g = 2.006$ (5 lines, $a_N = 7.2$ G).

Di-{4′-[2-(1-oxyl-3-oxide-4,4,5,5-tetramethylimidazoline)-phenyl]}phenylphosphine Oxide 2d. A solution of $NaIO_4$ (0.42 g, 2 mmol) in H_2O (10 mL) was added to a suspension of **2c** (0.38 g, 0.65 mmol) in CH_2Cl_2 (30 mL). The reaction mixture was stirred for 15 min, during which a deep blue color developed in the organic phase. The latter was collected, washed with H_2O, and dried over Na_2SO_4 before the solvent was removed in vacuo. The residue was purified by chromatography over silica (70−200 μm, 1.5 × 40 cm, eluent CH_2Cl_2−acetone 4/1). The main blue band was collected, and the solvent was removed in vaccuo. Compound **2d** was obtained as a blue crystalline solid by slow evaporation of a CH_2Cl_2−hexane solution. Anal. Calcd for $C_{32}H_{37}N_4O_5P$: C, 65.29; H, 6.33; N, 9.52. Found: C, 65.30; H, 6.57; N, 9.30. IR (KBr): 1420 (w), 1388 (m), 1364 (s), 1195 (m), 1133 (m), 829 (w), 710 (m), 616 (w), 566 (m), 2985 (w), 1434 (m), 1419 (s), 1388 (m), 1368 (s), 1303 (m), 1131 (m), 1089 (m), 697 (s). EPR (CH_2Cl_2, 293 K): $g = 2.006$ (5 lines, $a_N = 3.7$ G).

Tri-{4′-[2-(1-oxyl-3-oxide-4,4,5,5-tetramethylimidazoline)-phenyl]}phosphine Oxide 3d. A solution of $NaIO_4$ (0.39 g, 1.83 mmol) in H_2O (10 mL) was added to a suspension of **3c** (0.30 g, 0.47 mmol) in CH_2Cl_2 (25 mL). The reaction mixture was stirred for 15 min, during which a deep blue color developed in the organic phase. The latter was collected, washed with H_2O, and dried over Na_2SO_4 before the solvent was removed in vacuo. The residue was purified by chromatography over silica (35−70 μm, 1.5 × 40 cm, eluent CH_2Cl_2−acetone 7/3). The main blue band was collected, and the solvent was removed in vacuo to yield **3d** as a blue solid. Crystalline **3d** was obtained by slow evaporation of a CH_2Cl_2−CH_3CN solution. Anal. Calcd for $C_{39}H_{48}N_6O_7P$: C, 62.97; H, 6.50; N, 11.30. Found: C, 62.00; H, 6.47; N, 10.94. IR (KBr): 1426 (w), 1387 (m), 1358 (s), 1194 (m), 1111 (m), 710 (m), 618 (w), 566 (s). EPR (CH_2Cl_2, 293 K): $g = 2.006$ (13 lines, $a_N = 2.5$ G).

EPR Spectra. X-band (9.5 GHz) ESR spectra were recorded on a standard Bruker *cw* spectrometer of the ESP-300E series, equipped with a field-frequency (F/F) lock accessory and a built-in NMR Gaussmeter. A rectangular TE102 cavity was used for the measurements. The spectrometer was also equipped with a Bruker ER 4121 HT nitrogen cryostat controlled by an Oxford ITC4 temperature control unit. The signal-to-noise ratio of spectra was increased by accumulation of scans using the F/F lock accessory to guarantee large field reproducibility in each scan. Precautions to avoid undesirable spectral distortions and line broadenings, such as those arising from microwave power saturation and magnetic field overmodulation, were also taken into account. To avoid dipolar line broadening (from dissolved O_2), solutions were always carefully degassed three times using vacuum−thaw cycles with pure Ar. High-resolution isotropic ESR spectra were obtained by an optimal choice of the experimental conditions, temperature, viscosity, and radical concentration, that reduce the spectral line width to the minimum.[21] The optimal experimental conditions were as follows: moderate viscosities, $\eta \geq 25$ cP, intermediate temperatures, $220 \leq T \leq 300$ K, and low radical concentrations, $c \leq 5 \times 10^{-5}$ M. Computer simulations of experimental isotropic spectra were carried out with the EPRFTSM program.[64]

The frozen solution studies were recorded on a Bruker EMX spectrometer at X-band (9.3 GHz) equipped with an Oxford ESR-900 helium cryostat controlled by an Oxford ITC4 temperature control unit. Computer analysis of the experimental data was done with the Bruker WINEPR Simfonia program.

^{31}P and ^{1}H MAS NMR Spectra. The ^{31}P and ^{1}H MAS NMR spectra were recorded with a Bruker MSL 300 spectrometer by using microcrystalline samples of the compounds after mixing them in a glovebox with 8% of nickelocene, which was used as internal temperature standard.[34] Subsequently, the powder was packed into ZrO_2 rotors with 4 mm diameter and sealed with Kel-F caps. The free induction decays were sampled after applying single 90° pulses of 4 μs duration with a delay time of 100−500 ms between successive scans. Data handling included exponential multiplication up to the matched filter and baseline correction. The experimental signal shifts, δ^{exp}, were determined relative to external adamantane ($\delta(^1H) = 2.0$) and ammonium hydrogen phosphate (($\delta(^{31}P) = 1.1$ ppm). Contact shifts were obtained after subtracting the signal shifts, δ^{dia}, from the experimental signal shifts, δ^{exp}, of corresponding nuclei of diamagnetic reference compounds (triphenylphosphine oxide for **1d**, **2d**, and **3d** with $\delta(^{31}P) = 28.5$ ppm and $\delta(^1H) = 7.5$ ppm for all aromatic protons; triphenylphosphine for **1e** with $\delta(^{31}P) = -9.2$ ppm and $\delta(^1H) = 7.5$ ppm for all aromatic protons; and the pentacarbonylmolybdenum triphenylphosphine complex for **4** with $\delta(^{31}P) = 37.5$ ppm[65] and 1,3-dihydroxy-4,4,5,5,-tetramethyl-2-(3-pyridyl)-tetraimidazole for the proton signals of the radical imidazolyl moiety with $\delta(C^1H_3) = 1.1$ ppm). Note that the dipolar shift contribution can be neglected, because the g-factor anisotropy of organic radicals is generally very small.[66] Further details are given in Table S1 of the Supporting Information.

Theoretical Calculations. All calculations were done with the Gaussian 98[67] package on a Compaq ES40 parallel computer at the Max-Planck-Institut für Bioanorganische Chemie. The UB3LYP exchange-correlation functional[68,69] and the double ζ-quality Lanl2DZ basis set[70−73] were employed throughout, but some calculations were repeated at the 6-31G (C, H, N)/6-31+G* (P, O) level for selected molecules, because the 6-31+G* basis set includes diffuse functions said to be advantageous for calculations on compounds with lone pairs. Spin densities were calculated in single point runs at the crystal structure coordinates when available and on optimized geometry converged to the standard criteria. To obtain accurate energies for the calculation of the exchange coupling constants, a tight convergence criterion with the limit set to 10^{-8} and the ultrafine grid were used. No spin projection was used in the calculation of the exchange parameter as advocated by Ruiz et al.[74] The spin-Hamiltonian used to calculate the energy differences was

$\hat{H} = -2J\hat{S}_1\hat{S}_2$. The exchange parameter is then obtained as $J = {}^1/_2(E_S - E_T)$.

Acknowledgment. This work was supported by the European Union TMR Research Network ERB-FMRX-CT-98-0181 (1998-2003) entitled "Molecular Magnetism: From Materials toward Devices". U.S. and E.R. gratefully acknowledge Prof. Dr. K. Wieghardt for access to the computational facilities at the Max-Planck-Institut für Bioanorganische Chemie.

Supporting Information Available: Experimental details of the solid-state NMR measurements; spin densities computed and optimized geometries of **1d**, **1e**, **2d**, **3d**, and **5**, as well as of the hypothetical di- and tri-radical derivatives. This material is available free of charge via the Internet at http://pubs.acs.org.

References and Notes

(1) Amabilino, D. B.; Veciana, J. In *Magnetism: Molecules to Materials II*; Miller, J. S., Drillon, M., Eds.; Wiley-VCH: Weinheim, 2001; Vol. 2, pp 1−60.

(2) Itoh, K., Kinoshita, M., Eds. *Molecular Magnetism: New Magnetic Materials*; Gordon and Breach: Amsterdam, 2000.

(3) Lahti, P. M. *Magnetic Properties of Organic Materials*; Marcel Dekker: New York, 1999.

(4) Iwamura, H.; Inoue, K. In *Magnetism: Molecules to Materials II*; Drillon, M., Miller, J. S., Eds.; Wiley-VCH: Weinheim, 2001; Vol. 2, pp 61−108.

(5) Caneschi, A.; Gatteschi, D.; Lalioti, N.; Sangregorio, C.; Sessoli, R.; Venturi, G.; Vindigni, A.; Rettori, A.; Pini, M. G.; Novak, M. A. *Angew. Chem., Int. Ed.* **2001**, *40*, 1760−1763.

(6) Kumagai, H.; Inoue, K. *Angew. Chem., Int. Ed.* **1999**, *38*, 1601−1603.

(7) Sutter, J.-P.; Kahn, M. L.; Golhen, S.; Ouahab, L.; Kahn, O. *Chem.-Eur. J.* **1998**, *4*, 571−576.

(8) Fegy, K.; Luneau, D.; Ohm, T.; Paulsen, C.; Rey, P. *Angew. Chem., Int. Ed.* **1998**, *37*, 1270−1273.

(9) Fegy, K.; Sanz, N.; Luneau, D.; Belorizky, E.; Rey, P. *Inorg. Chem.* **1998**, *37*, 4518−4523.

(10) Caneschi, A.; Gatteschi, D.; Sessoli, R.; Rey, P. *Acc. Chem. Res.* **1989**, *22*, 392−398.

(11) Iwamura, H. I. K.; Hayamizu, T. *Pure Appl. Chem.* **1996**, *68*, 243−252.

(12) Inoue, K.; Hayamizu, T.; Iwamura, H.; Hashizume, D.; Ohashi, Y. *J. Am. Chem. Soc.* **1996**, *118*, 1803−1804.

(13) Matsuda, K.; Yamagata, T.; Seta, T.; Iwamura, H.; Hori, K. *J. Am. Chem. Soc.* **1997**, *119*, 8058−8064.

(14) Lahti, P. M.; Ichimura, A. S. *J. Org. Chem.* **1991**, *56*, 3030−3042.

(15) Rancurel, C.; Sutter, J.-P.; Kahn, O.; Guionneau, P.; Bravic, G.; Chasseau, D. *New J. Chem.* **1997**, *21*, 275−277.

(16) Rancurel, C.; Sutter, J.-P.; Le Hoerff, T.; Ouahab, L.; Kahn, O. *New J. Chem.* **1998**, 1333−1335.

(17) Leznoff, D. B.; Rancurel, C.; Sutter, J.-P.; Rettig, S. J.; Pink, M.; Paulsen, C.; Kahn, O. *J. Chem. Soc., Dalton Trans.* **1999**, 3593−3599.

(18) Leznoff, D. B.; Rancurel, C.; Sutter, J.-P.; Rettig, S. J.; Pink, M.; Kahn, O. *Organometallics* **1999**, *18*, 5097−5102.

(19) Rancurel, C.; Leznoff, D. B.; Sutter, J.-P.; Golhen, S.; Ouahab, L.; Kliava, J.; Kahn, O. *Inorg. Chem.* **1999**, *38*, 4753−4758.

(20) Rancurel, C.; Leznoff, D. B.; Sutter, J.-P.; Guionneau, P.; Chasseau, D.; Kliava, J.; Kahn, O. *Inorg. Chem.* **2000**, *39*, 1602−1605.

(21) Cirujeda, J.; Vidal-Gancedo, J.; Jürgens, O.; Mota, F.; Novoa, J. J.; Rovira, C.; Veciana, J. *J. Am. Chem. Soc.* **2000**, *122*, 11393−11405.

(22) Köhler, F. H. In *Magnetism: Molecules to Materials*; Miller, J. S., Drillon, M., Eds.; Wiley-VCH: Weinheim, 2001; Vol. 1, pp 379−430.

(23) Baldwin, R. A.; Cheng, M. T. *J. Org. Chem.* **1967**, *32*, 1572−1577.

(24) Ravindar, V.; Hemling, H.; Schumann, H.; Blum, J. *Synth. Commun.* **1992**, *22*, 841−851.

(25) Bartlett, P. A.; Bauer, B.; Singer, S. J. *J. Am. Chem. Soc.* **1978**, *100*, 5085−5089.

(26) Hoots, J. E.; Rauchfuss, T. B.; Wrobleski, D. A. *Inorg. Synth.* **1982**, *21*, 175−179.

(27) Jahn, W. *Z. Naturforsch.* **1989**, *44b*, 1313.

(28) Chalier, F.; Berchadsky, Y.; Finet, J.-P.; Gronchi, G.; Marque, S.; Tordo, J. *J. Phys. Chem.* **1996**, *100*, 4323−4330.

(29) Ullman, E. F.; Osiecki, J. H.; Boocock, D. G. B.; Darcy, R. *J. Am. Chem. Soc.* **1972**, *94*, 7049−7059.

(30) Wertz, J. E.; Bolton, J. R. *Electron Spin Resonance, Elementary Theory and Practical Applications*; Wiley and Sons: New York, 1994.

(31) Heise, H.; Köhler, F. H.; Mota, F.; Novoa, J. J.; Veciana, J. *J. Am. Chem. Soc.* **1999**, *121*, 9659−9667.

(32) Maruta, G.; Takeda, S.; Imachi, R.; Ishida, T.; Nogami, T.; Yamaguchi, K. *J. Am. Chem. Soc.* **1999**, *121*, 424−431.

(33) Heise, H.; Köhler, F. H.; Herker, M.; Hiller, W. *J. Am. Chem. Soc.* **2002**, *124*, 10823−10832.

(34) Heise, H.; Köhler, F. H.; Xie, X. *J. Magn. Reson.* **2001**, *150*, 198−206.

(35) Torssell, K. *Tetrahedron* **1977**, *23*, 2287−2291.

(36) Atherton, N. M. *Principles of Electron Spin Resonance*; Ellis Horwood Prentice Hall: New York, 1993.

(37) Weissman, S. L.; Kothe, G. *J. Am. Chem. Soc.* **1975**, *97*, 2537−2538.

(38) Wienk, M. M.; Jansen, R. A. *J. Am. Chem. Soc.* **1997**, *119*, 5398−5403.

(39) Deumal, M.; Lafuente, P.; Mota, F.; Novoa, J. J. *Synth. Met.* **2001**, *122*, 477−483.

(40) Rancurel, C.; Daro, N.; Benedi Borobia, O.; Hertweck, E.; Sutter, J.-P. *Eur. J. Org. Chem.* **2003**, 167−171.

(41) Kanno, F.; Inoue, K.; Koga, N.; Iwamura, H. *J. Am. Chem. Soc.* **1993**, *115*, 847−850.

(42) Neely, J. W.; Hatch, G. F.; Kreilick, R. W. *J. Am. Chem. Soc.* **1974**, *96*, 652−656.

(43) Davis, M. S.; Morokuma, K.; Kreilick, R. W. *J. Am. Chem. Soc.* **1972**, *94*, 5588−5592.

(44) Zheludev, A. B. V.; Bonnet, M.; Delley, B.; Grand, A.; Ressouche, E.; Rey, P.; Subra, R.; Schweitzer, J. *J. Am. Chem. Soc.* **1994**, *116*, 2019−2027.

(45) Jameson, C. J.; Gutowsky, H. S. *J. Chem. Phys.* **1969**, *51*, 2790−2803.

(46) McFarlane, W. *Proc. R. Soc. London, Ser. A* **1968**, *306*, 185−199.

(47) Gray, G. A.; Cremer, S. E. *J. Org. Chem.* **1972**, *37*, 3458−3469.

(48) McFarlane, W.; Rycroft, D. S. *J. Chem. Soc., Dalton Trans.* **1974**, 1972−1999.

(49) Bryce, D. L.; Eichele, K.; Wasylishen, R. E. *Inorg. Chem.* **2003**, *42*, 5085−5096.

(50) Anderson, P. W. In *Solid State Physics*; Seitz, F., Turnbull, D., Eds.; Academic Press: New York, 1963; Vol. 14, pp 99−214.

(51) Itoh, T.; Matsuda, K.; Iwamura, H. *Angew. Chem., Int. Ed.* **1999**, *38*, 1791−1793.

(52) Okada, K. In *Molecular Magnetism: New Magnetic Materials*; Itoh, K., Kinoshita, M., Eds.; Gordon and Breach: Amsterdam, 2000; pp 264−277.

(53) Liao, Y.; Baskett, M.; Lahti, P. M.; Palacio, F. *Chem. Commun.* **2002**, 252−253.

(54) Itoh, T.; Matsuda, K.; Iwamura, H.; Hori, K. *J. Am. Chem. Soc.* **2000**, *122*, 2567−2576.

(55) Brown, E. C.; Borden, W. T. *J. Phys. Chem. A* **2002**, *106*, 2963−2969.

(56) Mitsumori, T.; Inoue, K.; Koga, N.; Iwamura, H. *J. Am. Chem. Soc.* **1995**, *117*, 2467−2478.

(57) Borden, T. B.; Davidson, E. R. *J. Am. Chem. Soc.* **1977**, *99*, 4587−4594.

(58) Matsumoto, T.; Ishida, T.; Koga, N.; Iwamura, H. *J. Am. Chem. Soc.* **1992**, *114*, 9952−9959.

(59) Schatzschneider, U.; Weyhermüller, T.; Rentschler, E. *Eur. J. Inorg. Chem.* **2001**, 2569−2586.

(60) Schatzschneider, U.; Rentschler, E. *J. Mol. Struct. (THEOCHEM)* **2003**, *638*, 163−168.

(61) Lamchem, M.; Mittag, T. W. *J. Chem. Soc. C* **1966**, 2300−2303.

(62) Hirel, C.; Vostrikova, K. E.; Pécaut, J.; Ovcharenko, V. I.; Rey, P. *Chem.-Eur. J.* **2001**, *7*, 2007−2014.

(63) Schiemenz, G. P.; Kaack, H. *Liebigs Ann. Chem.* **1973**, 1480−1493.

(64) Kirste, B. EPRFTSM Program, Freie Universität, Berlin, 1991.

(65) Grim, S. O.; Wheatland, D. A.; McFarlane, W. *J. Am. Chem. Soc.* **1967**, *89*, 5573−5577.

(66) Kurland, R. J.; McGarvey, R. B. *J. Magn. Reson.* **1970**, *2*, 286−301.

(67) Frisch, M. J.; Trucks, G. W.; Schlegel, H. B.; Scuseria, G. E.; Robb, M. A.; Cheeseman, J. R.; Zakrzewski, V. G.; Montgomery, J. A., Jr.; Stratmann, R. E.; Burant, J. C.; Dapprich, S.; Millam, J. M.; Daniels, A. D.; Kudin, K. N.; Strain, M. C.; Farkas, O.; Tomasi, J.; Barone, V.; Cossi, M. R.; Cammi, R.; Mennucci, B.; Pomelli, C.; Adamo, C.; Clifford, S.; Ochterski, J.; Petersson, G. A.; Ayala, P. Y.; Cui, Q.; Morokuma, K.; Malick, D. K.; Rabuck, A. D.; Raghavachari, K.; Foresman, J. B.; Cioslowski, J.; Ortiz, J. V.; Baboul, A. G.; Stefanov, B. B.; Liu, G.; Liashenko, A.; Piskorz, P.; Komaromi, I.; Gomperts, R.; Martin, R. L.; Fox, D. J.; Keith, T.; Al-

Laham, M. A.; Peng, C. Y.; Nanayakkara, A.; Challacombe, M.; Gill, P. M. W.; Johnson, B.; Chen, W.; Wong, M. W.; Andres, J. L.; Gonzalez, C.; Head-Gordon, M.; Replogle, E. S.; Pople, J. A. *Gaussian 98*, revision A.7; Gaussian, Inc.: Pittsburgh, PA, 1998.

(68) Becke, A. D. *J. Chem. Phys.* **1993**, *98*, 5648−5652.

(69) Miehlich, B.; Savin, A.; Stoll, H.; Preuss, H. *Chem. Phys. Lett.* **1989**, *157*, 200−206.

(70) Dunning, T. H.; Hay, P. J. In *Modern Theoretical Chemistry*; Schaeffer, H. F., III, Ed.; Plenum: New York, 1976; Vol. 3, pp 1−27.

(71) Hay, P. J.; Wadt, W. R. *J. Chem. Phys.* **1985**, *82*, 270−283.

(72) Wadt, W. R.; Hay, P. J. *J. Chem. Phys.* **1985**, *82*, 284−298.

(73) Hay, P. J.; Wadt, W. R. *J. Chem. Phys.* **1985**, *82*, 299−310.

(74) Rodriguez-Fortea, A.; Alemany, P.; Alvarez, S.; Ruiz, E. *Chem.-Eur. J.* **2001**, *7*, 627−637.